7th International Conference on HYDROELASTICITY IN MARINE TECHNOLOGY
Split, Croatia, September 16th – 19th 2015

Coupled Fluid-Structure Interaction to model Three-Dimensional Dynamic Behaviour of Ship in Waves

P.A.Lakshmynarayanana[1], P.Temarel[1] and Z.Chen[1]

[1] Fluid Structure Interactions Group, University of Southampton, U.K

Abstract. Increase in computational power over the recent years has made it possible to investigate fluid-structure interaction problems using RANS/CFD and Finite Element software. However, the majority of these investigations are carried out using one-way coupling, thus omitting important fluid-structure interactions. A strong or two-way coupling between RANS/CFD and FEA is presented in this paper to model symmetric motion and response of flexible floating bodies in regular head waves. To illustrate this application, the RAOs of vertical displacements and wave-induced loads are calculated at various locations along a flexible three-dimensional barge (3-D) barge. The structure of the flexible barge is modelled as beam, in line with the flexible backbone model used in the experiments. The computational results are compared with experimental measurements and two-dimensional (2-D) linear hydroelastic predictions. A preliminary investigation for the static, still water, response of a flexible S-175 container ship model is also presented.

Keywords*: Hydroelasticity; Fluid-Structure interaction; RANS/CFD; wave-induced loads; Coupling; Modal superposition.*

1. Introduction

In the present study we focus our attention on fluid-structure interactions (FSI) of flexible floating bodies in waves by coupling CFD (Computational Fluid Dynamics) and FEA (Finite Element Analysis) software. Dynamics of structures or hydroelastic theories have to be taken into account when calculating motions and responses of 'softer' or flexible hulls owing to the increasing trend of the size of ships and offshore structures [1, 2]. In such cases, the response of the structure could significantly affect the flow field and fluid loading, resulting in a fully coupled system.

Hydroelastic investigations are predominantly experimental, using flexible backbone models, or numerical ranging from linear to partially nonlinear potential flow solvers [3, 4]. However, solving RANS (Reynolds-averaged Navier-Stokes) equations computationally to predict ship performance can be more efficient and realistic in some cases [5]. RANS/CFD can take into account nonlinearities associated with free surface flow, viscous effects, as well as local flow features [6].

The majority of investigations using RANS/CFD and FEA are carried out using one-way coupling, where the structural response of the structure does not affect the

fluid loading. However, a fully coupled CFD/FEA method has to be established to accurately model the responses of flexible floating bodies. Such investigations show promising results [7,8], but more is needed.

In this study a two-way coupling between a finite volume CFD method, using Star-CCM+ (version 8.04), and a finite element method (FEM), using Abaqus (version 6.13-1), is applied to assess the hydroelastic effects of a flexible barge in regular head waves. Thus, only symmetric distortions of the barge are calculated. 3-D computations are first carried out treating the barge as a rigid body to inform the modeling process. Star-CCM+ and Abaqus have inbuilt modules which makes it possible to couple them without any third party code. The barge is modelled as a non-uniform Timoshenko beam with properties as per the model test [9]. Numerical predictions are also obtained using 2-D hydroelasticity [10]. Predicted RAOs of vertical displacements at various locations along the barge are compared against experimental measurements. RAOs of vertical bending moment (VBM) and vertical shear force (VSF) predicted by the coupled CFD/FEM method are compared with 2-D hydroelastic results due to lack of experimental data. In addition the still water response of the coupled CFD/FEM model of the S-175 container ship is presented.

2. Numerical Method

2.1. Finite volume method

The numerical method used in Star-CCM+ is a finite volume (FV) method in which the flow is governed by RANS equations. In the case of an inviscid flow the RANS equations reduce to the well-known Euler equations, used in this paper. The fluid domain is discretized into a finite number of control volume (CVs). The discretized form of the governing equations is solved using a segregated iterative algorithm, called SIMPLE (Semi-Implicit Method for Pressure-Linked Equations). A detailed theoretical background is provided by Ferziger & Peric [11] .

Multiphase flows are implemented using the Volume of Fluid (VOF) tracking method. A sharp interface for free surface flows is maintained using the HRIC (High Resolution Interface Capturing) discretization scheme which is a blending of first and second order differencing scheme, and switched between them depending on the local Courant number.

The position of the body and the corresponding flow is updated at each iteration when the motion of the body at free surface is involved. The fluid grid is adjusted accordingly.

2.2. Grid adaptation and field data exchange in FSI

In the present study, grid adaptation to follow the motion of the body is implemented by two different methods, namely morphing and overset grids. Morpher collects a number of control points and their associated displacements to create an interpolation field and redistributes the mesh vertices.

An overset or overlapping grid consists of two regions; background and overset. The background grid is changed with changing wave length and height to include

refinements, in vertical and horizontal directions, required to maintain suitable mesh resolution. The overset grids are attached to the floating body and move with it. This method is highly efficient when compared to morphing in the case of free surface flows where the body undergoes large motion in waves.

In the case of rigid body simulations of the barge in head waves, grid adaptation has been carried out using overset grids. Both morphing and overset methods are applied to deform the grid in the two-way coupling. Morphing motion is set to the boundaries of the barge which deforms due to nodal displacements received from Abaqus. The overset grid boundaries move in response to the interpolation field created by the morphing motion using the "floating boundary condition" in the morpher.

The coupling is done by exchanging field data, i.e., pressure and nodal displacements between Star-CCM+ and Abaqus. Star-CCM+ uses the natural shape function of the FE topology to map the field data between fluid and structure grids.

2.3. Coupling scheme

The coupling scheme controls the sequence of data exchanges in the co-simulations. Star-CCM+ provides two coupling schemes, namely explicit and implicit coupling. In the explicit scheme, or loosely coupled problem, field data exchange takes place once every time step. In the implicit scheme field data is exchanged, by default, at every single iteration within a time step. Strong coupling is associated with dynamic problems where fluid loading and structural velocities change dramatically. The implicit scheme, being more stable, is ideal for such problems, but at a higher computational cost. The explicit scheme was tested with even very small time steps but resulted in pressure divergence; hence, the implicit scheme had to be used.

2.4. 2-D Hydroelastic analysis

Generalised coordinates for rigid and flexible modes of the barge are calculated using the 2-D hydroelasticity analysis by Bishop et al [10] . In brief, 2-D strip theory is used to calculate the hydrodynamic properties of the barge, using Lewis form representation. The barge structure is modelled as a Timoshenko beam. Modal summation is employed to represent vertical (or symmetric) displacement, bending moment and shear force at a specified location. The solution of the resultant unified equations of motion in regular waves provides the requisite generalized coordinates.

3. Response of a barge in regular waves

3.1. Barge characteristics and Test conditions

The experimental model of a flexible barge comprising 12 connected caissons is considered for validation of the present numerical method [13]. The flexible backbone structure of the barge has a $1cm^2$ square cross-section and is placed at 57 cm above deck level. All caissons are rectangular in shape, except for the bow caisson, which

has a beveled shape. Details of the experiments are described by Remy et al [9]. Table 1 shows the main particulars of the barge and the backbone.

The experimental measurements were carried out in regular (various headings) and irregular waves. Numerical simulations were carried out treating the barge as both rigid and flexible. Only regular head waves were chosen, as shown in Table 2, for validating the present numerical method, through comparisons with measured vertical displacements at: x/L: 0.08, 0.33, 0.5, 0.66, 0.83, 1.0, where x=0 denotes AP. The wave height (H) is 100mm for all except 50mm for 0.9s wave period. The rigid body modelling provided insight into domain size, damping zones and mesh refinement around the body and the free surface for each wave frequency. Numerical simulations were also carried out using 2-D hydroelasticity, providing the only comparator for VBM and VSF calculated using the co-simulation as these were not measured in the experiments.

Table 1. Main particulars of barge

Length of barge (caissons + clearance), L	2.445 m
Beam	0.6 m
Depth	0.25 m
Draft	0.12 m
KG	0.163m
Total mass (caissons + equipment)	172.53 kg
Bending stiffness of backbone (EI)	175 N m^2

Table 2. Domain sizes for regular wave periods and lengths used (* port side only)

Wave period (s)	Wave length (m)	Location of inlet (m)	Wake region (m)	Damping zone (m)	Side wall * (m)	Water depth (m)
1.8	5.058	7.6	10	7.6	8.0	4.0
1.6	3.996	6.0	8.0	6.0	8.0	4.0
1.2	2.248	5.0	5.0	3.5	8.0	4.0
1.05	1.711	5.0	5.0	3.5	8.0	4.0
1.0	1.561	5.0	5.0	2.0	8.0	4.0
0.9	1.264	5.0	5.0	2.0	8.0	4.0

3.2. Computational fluid domain and boundary conditions

The barge is aligned with the x-axis, with the stern at x=0, and y and z-axis in the athwarthships and vertical directions, respectively. The domain sizes for individual wave frequencies, for both rigid and coupled simulations, are shown in Table 2. A numerical beach of 1.5 λ (wavelength) is set at the outlet to reduce wave oscillations and prevent any reflections. Symmetry condition is used for the rigid body simulations, whereas full domain was modelled for the co-simulation cases. The

length of the side wall (y-direction) is fixed as 8m on one side of the barge for all cases, as per experiments.
Boundary conditions were specified to mimic conditions in a towing tank. At the velocity inlet boundary the kinematics of the wave, i.e. the position of the free surface and velocity of the first order wave as field functions are specified. At the outlet boundary, the hydrostatic pressure of the wave and position of the undisturbed free surface are specified. All other boundaries are set to no-slip wall condition. A detailed description of the computational domain, grid design and numerical settings are given by Lakshmynarayanana et al [13] .

3.3. Computational grid design

A combination of trimmer, extruder and overset mesh is used for all CFD simulations. The body and free surface grid refinement is identical for both rigid body and co-simulations for the same wave frequency. Cartesian grids aligned with the free surface are desirable for free surface applications using VOF multiphase flows. Trimmer mesher produces a base mesh of hexahedral cells aligned with the free surface and trims this base mesh at the input hull surface creating polyhedrons. Once the base mesh is created, the side wall, in y-direction, and the outlet is extruded using user specified extrusion parameters (i.e. number of layers, stretching ratio and extrusion length) to produce orthogonal cells. Nevertheless, the mesh growth was kept under 1.1 to prevent any numerical reflections arising due to sudden change in grid sizes between adjacent cells [14].
The grid was refined along the free surface region, close to the barge and in the wave radiation zone around the barge using volumetric controls, as shown in Figure 1 for 1.2s wave period.

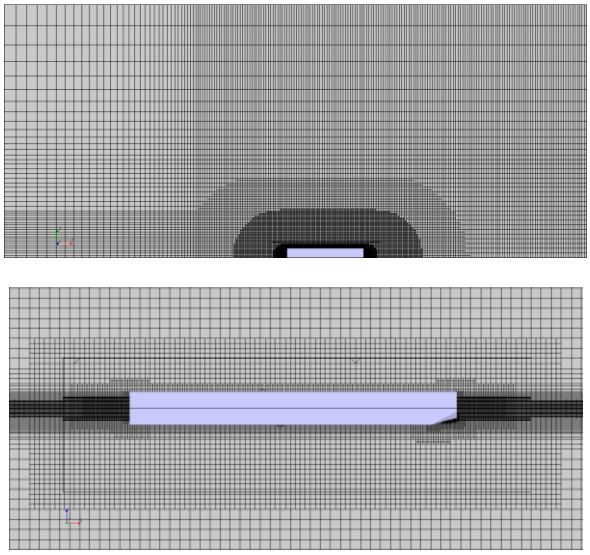

Figure 1. Grid refinement around the body and free surface for wave period of 1.2 s.

The waves radiated from the body form a circular wave contour in the bow and stern regions of the barge [15]. Hence, refinement around the body was also carried out to capture the disturbed wave pattern. In the free surface region, 45-60 cells are placed per wavelength and 12-15 cells per wave amplitude. Around 320 cells per wavelength and 160 cells per wavelength are clustered close to the barge and the wave radiation zone, respectively. The global mesh count for the co-simulation case varied from 2.3 million to 13.6 million. With grids of this size one can hardly find mesh sensitivity analyses in the literature on wave-body interactions. Nevertheless, Kim et al [16] performed convergence analysis for the radiation problem of a uniform flexible barge and concluded that the refinement effects were not significant except for very low frequencies of oscillation.

3.4. Solution strategy and numerical settings

Computations for both models were carried out using inviscid fluid model with an implicit unsteady solver. Temporal discretization and convection of segregated flow solver and VOF solver are 2^{nd} order accurate. Time step for the simulations were chosen such that the Courant number on the free surface at all times is less than 0.5. Iterative Implicit coupling scheme was chosen for the coupled simulations.

In the case of rigid body, body release and ramp times were specified based on the time step. It is best to allow the fluid flow to initialize and become steady before the calculation of body motions commences. A value of 50 time steps is specified as a release time. To minimize the effect of suddenly applied forces at release time, and facilitate a more robust solution by reducing oscillations, a ramp time equal to 10 times release time is specified.

The time-step size for both fluid and structural models in the co-simulation was the same. 12 inner iterations per time-step were used in the fluid solver and 2 iterations per data exchange were performed, different from the default in section 2.3, resulting in a total of 6 exchanges. The co-simulation displacement residuals reduced by an order of 4 at every time-step.

All simulations were run in parallel mode with single precision on the University of Southampton High Power Computing facility Iridis 4. It consists of a total of 12320 cores with each node containing 16 cores of 2.6GHz processing speed and 4GB RAM. For the co-simulations, the CPU hour for 1 sec of real time simulations varied from 35 hours to 126 hours, depending on the total mesh size.

3.5. F.E model

The flexible backbone is modelled using 48 2-node linear B31 beam elements in Abaqus 6.13-1. The beam elements are linked to dummy surface elements, 4-node quadrilateral SFM3D4, that represent the actual wetted surface of the barge. B31 is a Timoshenko beam element allowing for shear deformation. The shear stiffness evaluated by Abaqus based on the cross-section. Surface elements have no inherent stiffness but may have mass/unit area, though none is specified in this case. The dummy surface elements are linked to the nodes on the beam elements using kinematic coupling constraints, as shown in Figure 2. All six degrees of freedom are

constrained in the kinematic coupling of beam nodes and the dummy surface, in the sense that the beam deformations are imparted on to the barge hull. The total mass of the barge is distributed on the beam elements as non-structural mass. The responses in waves are evaluated using two-way coupling between CFD and FEA. The solution for displacements, deformations, stresses and forces in ABAQUS is carried out using the virtual work principle. In the case of beam elements bending moments and shear forces are obtained from the stresses.

In 2-D hydroelastic analysis, the non-uniform beam is divided into 48 sections, to achieve consistency with the FE model. The mass distribution, moment of inertia for each segment, is similar to the FE model. Rotary inertia is assumed to be zero. The responses in waves are evaluated using modal analysis [1].

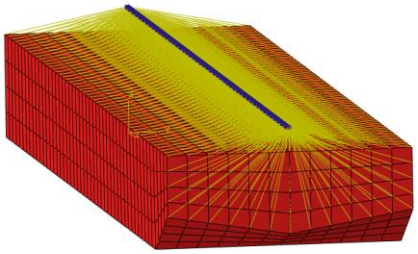

Figure 2. FE mesh: beam and dummy surface elements linked using kinematic coupling.

4. Results

4.1. Modal Analysis and free motion

Modal analysis was performed in Abaqus using the Block Lancozs eigen value extraction method. The natural frequencies and mode shapes obtained in Abaqus were compared to 2-D hydroelasticity calculations which use the finite difference (FD) method. The dry hull natural frequencies for the 2-node mode shape are 6.01 rad/s and 6.03 rad/s, for Abaqus and FD, respectively. The corresponding values for the 3-node mode shape are 16.43 rad/s and 16.49 rad/s.

A free decay test was simulated for the flexible barge to compare the wet natural requency of the barge with the experiments. For this test, the barge was initially inclined at 5 degrees to the still water line in both CFD and FE models. The Power Spectral Densities of the time histories of vertical displacement at the bow, amidships and the stern were obtained. The corresponding wet natural frequency for the 2-node mode is 6.2 rad/s and compares well with 5.9 rad/s obtained in the experiments.

4.2. Dynamic response of the barge

The responses of the barge treated as rigid and flexible body in regular head waves are presented in this section. Wave elevations were recorded at distance L in front of the barge. Average wave amplitude over 8-10 wave periods was used to calculate the RAOs. The maximum decrease in wave height for this window was only around 5-

6%. The rigid and hydroelastic predictions are distinguished by RIGID and FLEX, respectively, in Figure 3. Predictions from CFD simulations (rigid and flexible) and 2-D hydroelasticity are denoted by STAR and MARS, respectively. Coupled simulations using wave heights in Section 3.1 is denoted by STAR_FLEX_0.1. It should be noted that the experimental values contain both rigid displacement and deformation.

4.2.1. Vertical displacements in waves

In general, the rigid body response predicted by 2-D hydroelasticity compares well with the CFD results. However discrepancies were noted, especially towards the forward part of the barge – see Figure 3(d). The predicted rigid body displacements at amidships show very good agreement. At the forward section, strong bow waves were seen to develop in the CFD simulations, influenced by pitch motion, from a wave frequency of 3.93 rad/s and upwards, shown in Figure 4. With increase in frequency, diffraction becomes more dominant resulting in strong localized bow waves which is not well predicted by the 2-D linear analysis. The predictions using CFD is considered more reliable at forward and stern locations as it accounts for the nonlinear interaction and 3-D effects between wave and body - a drawback of 2-D strip theory.

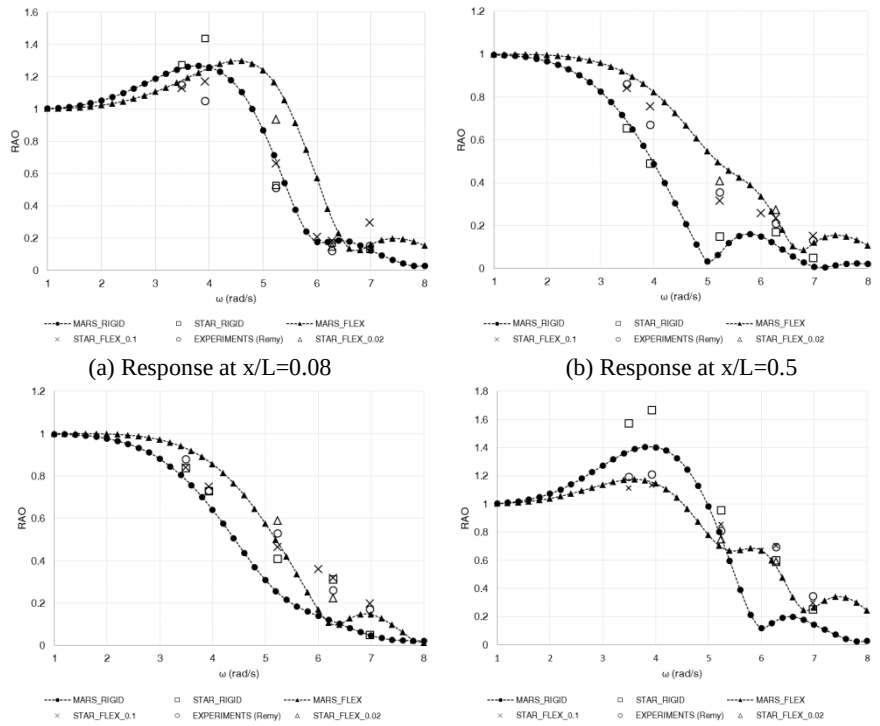

(a) Response at x/L=0.08 (b) Response at x/L=0.5

(c) Response at x/L=0.66 (d) Response at x/L=1.0

Figure 3. RAOs of vertical displacement along the barge at x/L=0.08, 0.5, 0.66, 1.0 from AP

RAOs from the CFD/FEM co-simulation, shown also in Fig.3, compare very well with the experimental measurements, especially from amidships to the forward end of the barge. The present method overpredicts the distortion at the aft end and amidships when compared with the experiments; maximum difference 15%. A grid convergence study is not conducted in the present simulations. Investigations using a finer mesh need to be carried out, in the future, to observe their effect on the solution.

2-D hydroelastic and CFD/FEM coupled predictions show fair agreement, although differences, of the order of 50%, can be observed at higher frequencies. The difference is attributed to strong diffraction effects at higher frequencies also prevalent in flexible body motions, albeit at higher frequencies as shown in Figure 5. Of the two numerical methods, predictions using CFD coupling show much better agreement with experimental data. The ratio H/L≈1/25 possibly resulting in significant nonlinear effects. To linearize the problem and make the comparison with 2-D linear predictions more realistic, a smaller wave height of 20 mm (H/L=1/122) was tested for 5.24 rad/s and 6.28 rad/s in the coupled CFD/FEM simulations, denoted as STAR_FLEX_0.02. The displacements at most locations for the coupled cases now shift towards the 2-D linear hydroelastic predictions, resulting in better agreement. Although a small difference still exists between the two numerical methods, it is evident that magnitude of nonlinearities is one of the main reasons for the discrepancy in the previous cases.

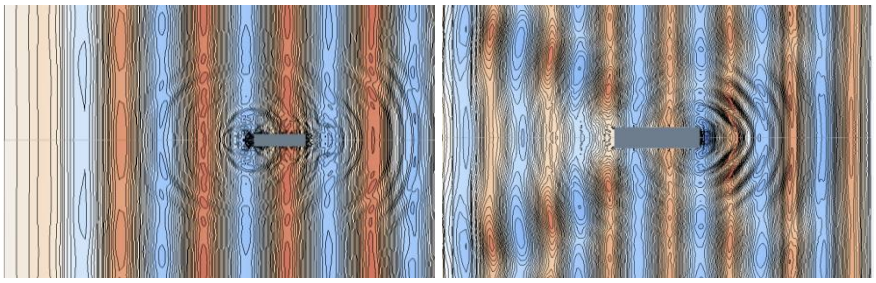

(a) (b)

Figure 4. Wave contours around the rigid body for (a) 3.93 rad/s at 11.5s (b) 6.28 rad/s at 9.5 s

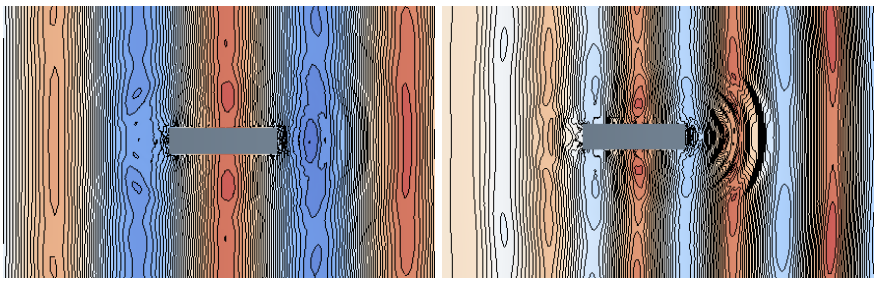

(a) (b)

Figure 5. Wave contour around flexible body for (a) 3.93 rad/s at 11.5s (b) 6.28 rad/s at 9.5 s

4.2.2. Vertical bending moment and shear force in waves

RAOs of VBM and VSF are shown in Figures 6 and 7, together with comparisons from 2-D hydroelasticity analysis. As can be seen from Figure 6, the first resonant peak is observed around 5.5 rad/s, which corresponds to λ/L=1 or ship-wave matching. In general, there is a fair agreement in RAO VBM, except at 5.24 and 6.28 rad/s, where the coupled CFD/FEM predictions are much smaller than 2-D linear predictions. To minimize the effects of nonlinearity, calculations were carried out for a wave height of 20mm at 5.24 rad/s and 6.28 rad/s and 10mm at 5.24 rad/s. For these cases, an increase in VBM at amidships and at 0.66L is observed, also observed in the corresponding displacements in Figure 3 when wave height was reduced. This still leaves a difference of about 30% between the 2-D linear and CFD/FEM predictions at amidships. No significant improvement is observed at the other two locations. Whilst examining the attitude of the barge in waves relatively large displacements in the longitudinal direction were observed. More investigations on the effect of this unphysical "head reach" on the VBMs (and VSFs) is required.

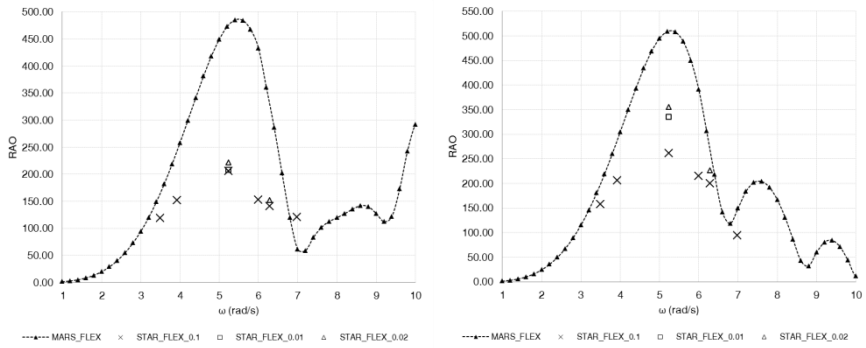

(a) Response at x/L= 0.33 (b) Response at x/L= 0.5

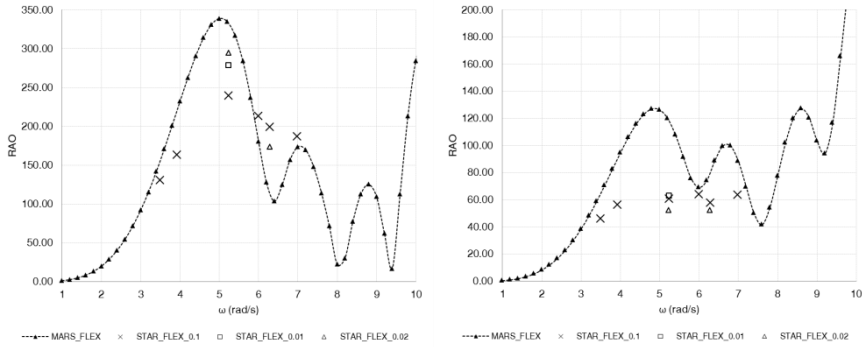

(a) Response at x/L= 0.66 (b) Response at x/L= 0.83

Figure 6. RAOs of VBM along the barge for the flexible body analysis.

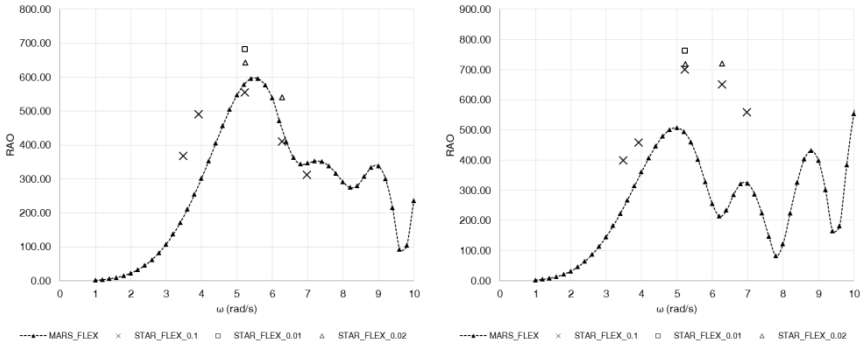

(a) Response at x/L= 0.33 (b) Response at x/L= 0.83

Figure 7. RAOs of VSF along the barge at x/L= 0.33 and 0.83 for the flexible body analysis.

The RAO VSF, shown in Figure 7, also show differences between the 2-D linear and coupled CFD/FEM predictions, of the order of 30%, the only exception being the stern location at x/L=0.08. No improved agreement could be obtained from the coupled CFD/FEM simulations with smaller wave heights. Lack of experimental data makes it difficult to reliably conclude as to which method is more accurate.

4.2.3. Response of the flexible barge in still water

The still water response of the barge was co-simulated and compared again with 2-D predictions, to shed light in the differences observed in waves. The static responses for the coupled CFD/FEM case were calculated after the forces and displacements had attained a steady value in the time domain. The still water VBM and deflection are shown in Figure 8. The 2-D VBM is obtained using net load integration and modal summation, denoted as STATIC and MODAL, respectively. As can be seen the static VBM predicted by coupled CFD/FEM is 12 times larger than the 2-D static analysis. At the forward end of the barge, a high non-zero moment is also noted in the coupled simulation, which for a free-free beam must be close to zero. Even the deflections along the length are over predicted.

In the original FE model, shown in Figure 3, the number of beam nodes and longitudinal sections on the dummy surface were the same. To investigate the effect of a finer FSI surface, the longitudinal sections were doubled and each beam node was now linked to two longitudinal sections of the hull surface. The results are denoted as STAR_FLEX_REFINED in Figure 8 and show no improvement.

The overall predicted static deflection is approximately 1 and 2cm, for the 2-D and coupled CFD/FEM methods. This is equal to or twice the backbone height , which is 1cm. Coupled CFD/FEM simulation was run using 10 times larger bending stiffness than that shown in Table 1, to assess sensitivity of VBM to deflection, denoted by STIFF. Furthermore, a uniform stiff rectangular barge was also co-simulated, denoted by RECT_STIFF. The stiffer barge has deflections and VBM much closer to the 2-D predictions and the uniform stiffer barge also has nearly zero VBM at FP. This analysis illustrates that there may be particular issues when evaluating loads using coupled CFD/FEM for this very flexible and nearly uniform barge.

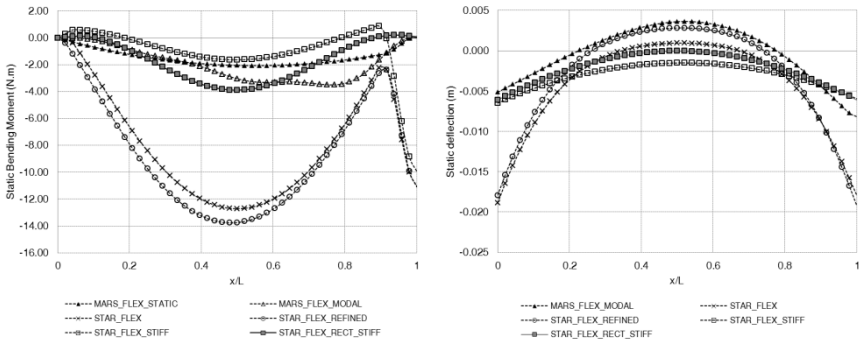

(a) Bending moment (b) Static deflection

Figure 8. Still water bending moment and deflection of the flexible barge

4.3. Still water response of S-175 container ship

The coupled CFD/FEM method is next applied to the S-175 containership model [17]. Due to the problems experienced with the barge in still water, the static response of S-175 was compared with 2-D method. The CFD and FE modeling follows the same process described in Sections 3.3 to 3.6 and the backbone properties are obtained from Wu & Hermundstad [18] using 20 beam elements and 9908 dummy surface elements. The CFD and FE models are shown in Figure 9, the former comprising of 700,000 cells. The predicted static VBM and VSF, shown in Figure 10, agree well with each other.

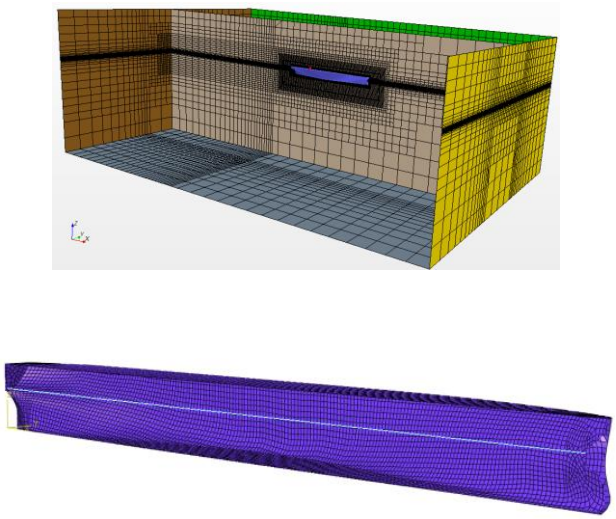

Figure 9. CFD and FE mesh for the S-175 containership

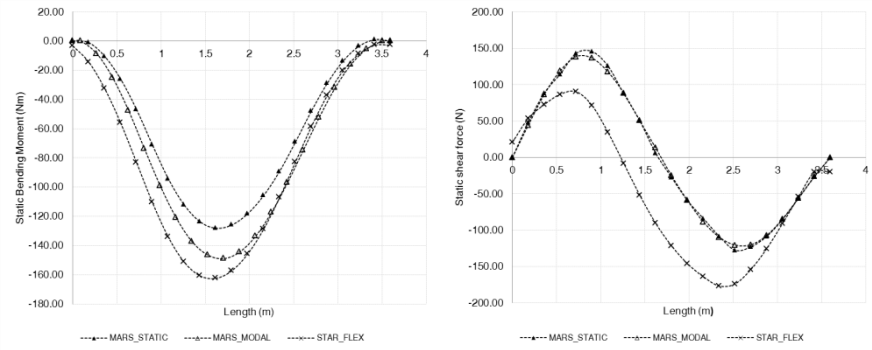

(a) Bending moment (b) Shear force

Figure 10. Still water bending moment and shear force for S-175 containership

5. Conclusions

The principal aim of this paper is to apply a coupled time domain CFD/ FEM analysis to investigate hydroelastic response of bodies in waves. This is achieved using commercially available software Star-CCM+ and Abaqus. The target application is the simulation of flexible barge in regular head waves. Calculations were carried out for both rigid body and flexible structural idealisations.

Very good agreement is achieved for the RAOs of vertical displacement between the CFD/FEM coupling and experimental measurements in most cases, with some exceptions especially at the forward sections of the barge. Differences observed between the coupled CFD/FEM simulations and 2-D linear predictions are mainly attributed to the influence of strong bow and stern waves systems, nonlinearities and 3-D effects. RAOs of VBM and VSF in waves using the two numerical predictions showed significant differences, especially in way of ship-wave matching region. Co-simulations carried out using small wave heights, to linearize the response, showed slight variation in VBM amidships indicating the influence of nonlinearities. Nevertheless, the difference in bending moment amidships was about 30%; the coupled CFD/FEM method predicting smaller response.

Still water VBMs calculated using CFD/FEM coupling showed significant dependence of the VBM on the magnitude of barge stiffness, hence deformation. It is believed that this may be due to this barge being very flexible, rather than a generic issue in the coupled CFD/FEM method. A preliminary investigation of still water VBMs for the S-175 containership showed promising results.

The results presented show that the coupling technique investigated is reliable and compares well with experimental displacements for a flexible barge. Discrepancies are observed between CFD/FEM coupling and 2-D hydroelastic predictions for bending moments and shear forces. An attempt has been made to explain the reason for these differences; however, lack of experimental data for the barge makes verification difficult. Further investigations are required, e.g. along the lines suggested in section 4.2.2. It is worth noting that investigations on FSI using CFD and FEA, e.g. [5, 7 and 8] perform the coupling between CFD and a solver based on

modal analysis rather than FEA. Co-simulation of the S-175 containership and comparison with available experimental measurements will follow.

Acknowledgements

The authors acknowledge the support of The Lloyd's Register Foundation through its University of Southampton Technology Centre and Lloyd's Register . The authors also thank Professor Molin and Mr. Remy for providing experimental data.

References

[1] Bishop, R.E.D. & Price, W.G., 1979. *Hydroelasticiy of Ships*, Cambridge University Press.
[2] Bishop, R.E.D., Price, W.G. & Wu.Y, 1986. A general linear hydroelasticity theory of floating structures moving in a seaway. *Phil. Trans. R. Soc. London*, A316, pp.375–426.
[3] ISSC., 2012. Report of Committee I.2: Loads. *In Proceedings of the 18th International Ship and Offshore Structures Congress, Rostock*, Germany. 1, pp.79–150.
[4] ITTC, 2014. The Seakeeping Committe final report and recommendations. *In the Proceedings of 26th ITTC*, Copenhagen.
[5] Piro, D.J. & Maki, K.J., 2013. Hydroelastic analysis of bodies that enter and exit water. *Journal of Fluids and Structures*, 37, pp.134–150.
[6] Querard, A.B.G., Temarel, P. & Turnock, S.R., 2009. The hydrodynamics of ship-like sections in heave, sway, and roll motions predicted using an unsteady Reynolds averaged Navier–Stokes method. In*: J. Engng Maritime Environment*, pp.227–238.
[7] Seng, S., Andersen, I.M. V & Jensen, J.J., 2012. On the influence of hull girder flexibility on the wave induce bending moments. *Hydroelasticity in Marine Technology*. pp. 341-353.
[8] Oberhagemann, J., Kromer, M., Cabos, C. & El Moctar, O., 2012. A fluid-structure coupling method based on field methods and a structural mode decomposition. *Hydroelasticity in Marine Technology*. pp. 267–276.
[9] Remy, F., Moilin, B. & Ledoux, A., 2006. Experimental and numerical study of wave response of a flexible barge. *Hydroelasticity in Marine Technology*. pp. 255–264.
[10] Bishop, R.E.D., Price, W.G. & Tam, P.K.Y., 1977. A unified dynamic analysis of ship response to waves. *Trans. R. Inst Nav. Architects*, 119, pp.363–390.
[11] Ferziger, J.. & Peric, M., 2003. *Computational Methods for Fluid Dynamics 3rd Edition*., Springer, Berlin.
[12] Malenica, S., Moan, B., Remy, F. & Senjanovic, I., 2003. Hydroelastic reponse of a barge to impulsive and non-impulsive wave loads. *Hydroelasticity in Marine Technology*. pp. 107–115.
[13] Lakshmynarayanana, P., Temarel, P. & Chen, Z., 2015. Hydroelastic analysis of flexible barge in regular waves using coupled CFD-FEM modelling. *In MARSTRUCT*. pp. 95–103.
[14] STAR-CCM+, 2012. STAR-CCM+ version 8.04 manual.
[15] Kim, Y. & Kim, K.H., 2009. Analysis of Hydroelasticity of Floating Shiplike Structure in Time Domain Using a Fully Coupled Hybrid BEM-FEM. *J. Ship Res.*, 50(1), pp.31–47.
[16] Kim, J. H., Lakshmynarayanana, P., & Temarel, P. (2014). Added mass and damping coefficients for a uniform flexible barge using VOF. In ICHD.
[17] Wu, Y., Chen, R. & Lin, J., 2003. Experimental Technique of Hydroelastic Ship Model. *Hydroelasticity in Marine Technology*. pp. 131–142.
[18] Wu, M. & Hermundstad, O.A., 2002. Time-domain simulation of wave-induced nonlinear motions and loads and its applications in ship design. *Marine Structures*, 15(6), pp.561–597.